Crystal truncation rods and surface roughness

I. K. Robinson
AT&T Bell Laboratories, Murray Hill, New Jersey 07974
(Received 13 September 1985)

We present x-ray-diffraction profiles from a variety of different crystals which are characteristically diffuse in the direction perpendicular to the surface through which the incident and diffracted beams pass, but sharp in both parallel directions. We show that these effects arise from truncation of the crystal lattice at the surface. To explain the precise form of the momentum-transfer dependence of the intensity across the reciprocal-space zone, it is necessary to include the effects of surface roughness on an atomic scale. Such measurements therefore allow highly sensitive roughness determinations to be made. Understanding the origin of these streaks of intensity will have significant impact on the practice of x-ray crystallographic determinations of surface structure.

In the classical derivation of the diffraction pattern of a crystal lattice, it is frequently assumed that the crystal is infinite in extent; the diffraction peaks are then perfect δ functions. When finite-size effects are included, the peaks are found to be broadened by an amount inversely related to the dimension of the diffracting region of the crystal. An often overlooked consequence of finite-size broadening is that, for a crystal with sharp boundaries, a significant amount of intensity is always scattered *far* away from the Bragg peaks and is spread right across the Brillouin zone. The order of magnitude of this intensity is the same as that arising from a single (crystalline) layer of atoms, and so x-ray experiments with monolayer sensitivity (now possible[1]) are able to detect it. We report and explain such measurements here.

A primitive parallelepiped crystal of dimensions N_1, N_2, and N_3 unit cells with lattice parameters a_1, a_2, and a_3 diffracts x-rays with an intensity proportional to the square of the structure factor,[2]

$$|F(q_1,q_2,q_3)|^2=\left|\sum_{j_1=1}^{N_1}\sum_{j_2=1}^{N_2}\sum_{j_3=1}^{N_3} e^{i(q_1a_1j_1+q_2a_2j_2+q_3a_3j_3)}\right|^2 =\frac{\sin^2(\frac{1}{2}N_1q_1a_1)}{\sin^2(\frac{1}{2}q_1a_1)}\frac{\sin^2(\frac{1}{2}N_2q_2a_2)}{\sin^2(\frac{1}{2}q_2a_2)}\frac{\sin^2(\frac{1}{2}N_3q_3a_3)}{\sin^2(\frac{1}{2}q_3a_3)} . \quad (1)$$

When N_1, N_2, and N_3 are large, the function is sharply peaked at the Bragg points where the intensity is $(N_1N_2N_3)^2$. The three Laue conditions for this are $q_1a_1=2\pi h$, $q_2a_2=2\pi k$, and $q_3a_3=2\pi l$, which define the reciprocal lattice. If one of these conditions is relaxed, say on q_3, the intensity tends in the limit of large N_3 to

$$|F(2\pi h/a_1,2\pi k/a_2,q_3)|^2=N_1^2N_2^2\frac{\sin^2(\frac{1}{2}N_3q_3a_3)}{\sin^2(\frac{1}{2}q_3a_3)} \to N_1^2N_2^2\frac{1}{2\sin^2(\frac{1}{2}q_3a_3)} \text{ as } N_3\to\infty \text{ for } q_3a_3\neq 2\pi l \quad (2)$$

where the rapid oscillations of the numerator are averaged out in the limit. Similar results can be readily obtained by relaxing the conditions on q_1 or q_2. Thus the diffraction intensity of the finite-sized crystal has diffuse streaks connecting all the Bragg points. The diffuse intensity far from the nodes is of order of magnitude N^4 compared with N^6 at the nodes.

Scattering that is sharp in two directions and diffuse in the third (referred to as a "rod" of scattering) must arise from a crystalline object that is localized in one dimension and extended in the other two. The two-dimensional objects in the problem under consideration are the *faces* of the parallelepiped crystal. The momentum transfer dependence in Eq. (2) is understood from the fact that the Fourier transform of a step function is $1/q$, which gives the $1/(\Delta q)^2$ dependence of the intensity near each of the Bragg points. The experimental configuration we wish to consider is that of a semi-infinite crystal measured with incident and diffracted beams passing through its surface. This is commonly called the "Bragg geometry." In this case five of the six faces of the parallelepiped become indistinct: four because of the edges of the beams are soft

 ©1986 The American Physical Society

(in practice) and the fifth because of the limited penetration of the beam. The Fourier transform of a broadened step function decays in reciprocal space much faster than $1/q$, so the diffuse rods of intensity due to the five soft faces retract to be localized in reciprocal space at or very close to the Bragg points. We are then left with only the sixth component due to the sharply truncated surface. We will call these features "crystal truncation rods."

We now wish to estimate the strength of the truncation rods in the Bragg geometry. We must first modify Eqs. (1) and (2) by including the x-ray coherence length, m (measured in unit cells), of the experimental configuration. This broadens all the diffraction features to $1/m$ reciprocal units. The Bragg points then have intensity of order $N_1N_2N_3m^3$, while the diffuse intensity is $N_1N_2m^2$. A typical penetration depth is 1 μm so $N_3 \approx 10^3$ unit cells (perpendicular to the face). With $m \sim 100$ unit cells, this gives a relative intensity

$$\frac{I(\text{Bragg point})}{I(\text{truncation rod})} = N_3 m \sim 10^5 .$$

In a careful experiment with a dynamic range better than 10^5, the diffuse scattering of the truncation rod perpendicular to the crystal face (Bragg geometry) should be measurable. It should also be noted that the diffuse intensity, of order $N_1N_2m^2$ far from the Bragg points, is independent of the number of layers penetrated into the crystal (N_3). Moreover, $N_1N_2m^2$ is precisely the intensity of the two-dimensional diffraction rods that arise from a *single layer* of $N_1 \times N_2$ atoms at the surface of the crystal.

Experimental observations of truncation rods are shown in Figs. 1—4. In Fig. 3, the full intensity of the Bragg peaks is recorded and seen to be $\sim 10^5$ times larger than the rods as expected. The four materials chosen as samples, Si, Pt, W, and InSb, represent metals and semiconductors, elements and compounds; their general surface properties are widely different from each other. Crystals were accurately aligned to a low-index surface plane and are designated by that plane. The methods of measurement were quite different in the different cases: for Pt(111) in Fig. 1 and W(100) in Fig. 3, a 60 kW rotating anode source, pyrolytic graphite monochromator, four-circle diffractometer, graphite analyzer, and scintillation counter were used to obtain very high signal to background with modest resolution.[1] For InSb(111) in Fig. 2 synchrotron radiation from the DORIS (Doppel-Ring Speicheranlage) storage ring at the Hamburger Synchrotronstrahlungslabor (HASYLAB) at Deutsches Elek-

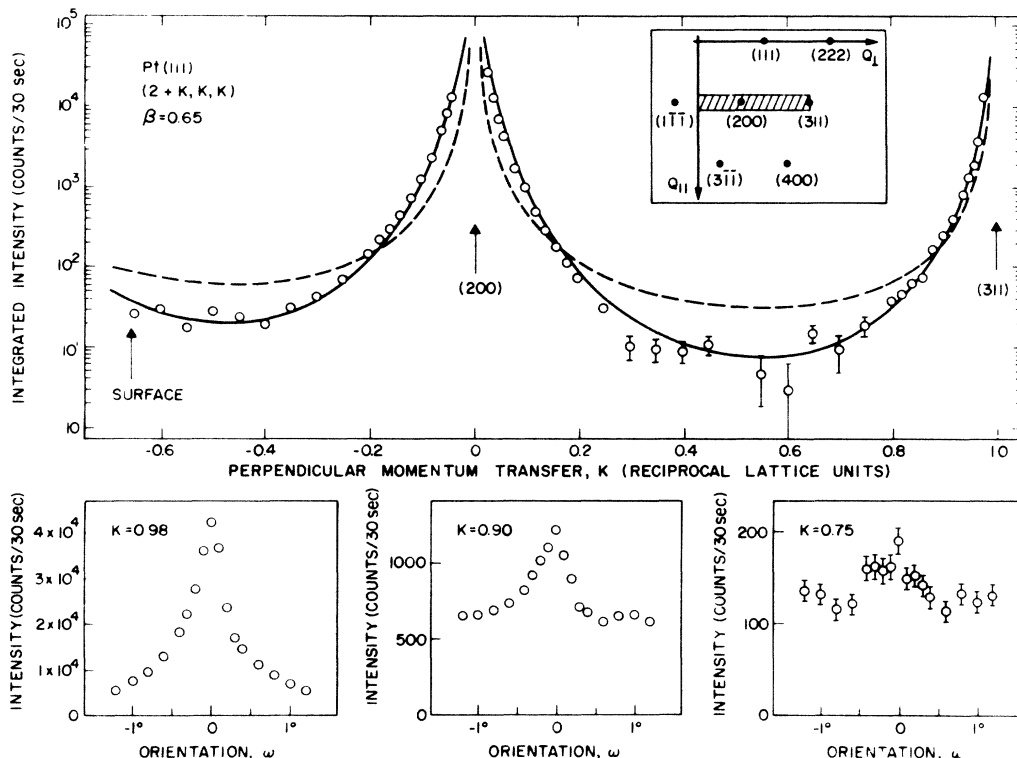

FIG. 1. Crystal truncation rod perpendicular to the (111) face of an etched Pt crystal under a He atmosphere. Measurements were made with a rotating anode source and four-circle diffractometer. The shaded bar on the reciprocal-space diagram inset shows the range of the scan which passes through two bulk Bragg reflections. Each point shown has been integrated over its rocking curve, has the thermal diffuse background subtracted, and has been corrected for Lorentz $\{[\sin(2\theta)]^{-1}\}$ and polarization $\{\cos^2(2\theta)+1\}$ factors. The bulk peaks have an intensity around 10^7 on the scale shown, but have been suppressed because of difficulty in removing the background reliably. Superimposed on the data are fits of truncation rods both with [solid line, Eq. (3)] and without roughness [dashed line, Eq. (2)]. Below are typical rocking scans showing that the rod is peaked above background at different positions.

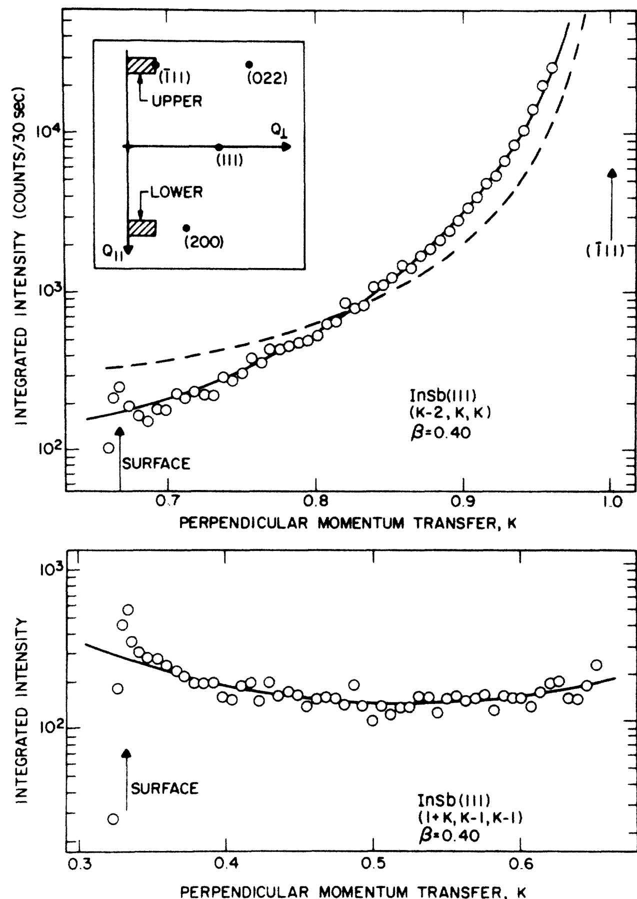

FIG. 2. Crystal truncation rods for InSb(111) in ultrahigh vacuum (UHV). The sample was prepared by sputtering and annealing for several hours, then transferred in UHV to a diffraction cell (Ref. 3). Synchrotron radiation at HASYLAB and a position sensitive detector oriented along the rod were used. The ω-integrated curve was accumulated in a parallel fashion by rotating the sample at constant velocity while the detector was running. Shaded bars on the inset mark the two scans shown, which are related by a 180° rotation of the crystal about its surface normal. The resolution-limited edge on the left-hand side of the scans marks the position of the surface: below it, the crystal blocks rays from reaching the detector. Just above the edge is the intensity enhancement expected for rays leaving the crystal close to the critical angle for total external reflection (Ref. 15). This small region of each curve has been omitted from the present fitting procedure but is described elsewhere (Ref. 16). Fits are shown for Eq. (2) (dashed line, no roughness) and Eq. (3) (solid line, with roughness).

tronen-Synchrotron (DESY) was used with a double Ge(111) monochromator, plane Au filter mirror, two-circle goniometer, and a position-sensitive proportional counter; even though no analyzer was used, background was low because the entire divergence of the incident beam was held within 5% of the critical angle for external reflection.[3] For Si(111) in Fig. 4 the focused wiggler beam line at Stanford Synchrotron Radiation Laboratory (SSRL) was used with a double asymmetric-cut Ge(111) monochromator, four-circle diffractometer, 0.5° Soller slits, and scintillation counter.[4] The W(100), InSb(111), and Si(111) samples were in ultrahigh-vacuum (UHV) environmental cells: the Si(111) and W(100) (Ref. 5) were cleaned by sublimation at 1450 and 2500 K, respectively; the InSb(111) was cleaned by sputtering and annealing at 700 K.[3] The Pt(111) sample was mechanically polished, etched in boiling aqua regia, electrochemically etched for 5 h, then annealed at atmospheric pressure under I_2 vapor in Ar at 600 K for 10 min and transfered through air to a He environment.[6]

Thermal diffuse scattering (TDS) has a functional form similar to Eq. (2), except that it is diffuse in all *three* reciprocal-space directions, and not concentrated along rods as are the truncation effects we are concerned with. The TDS is readily seen at the bottom of Fig. 1 as a background in scans of the sample orientation angle ω. These data, in which the TDS intensity is comparable with that of the truncation rod, were taken at positions along the rod *far* from the surface plane where the incident and diffracted x-ray beams subtend large angles with the surface and the penetration depth into the bulk is largest (see Fig. 1 inset). Close to the surface plane, where glancing incidence conditions exist, the TDS background was much reduced. Appreciable TDS was seen only for Pt(111) and W(100); the semiconductor samples, having large Debye temperatures and measured at high-resolution synchrotron radiation sources, showed negligible amounts. Nevertheless, the rod profiles of Figs. 1, 2, and 4 are ω integrated and background subtracted, point by point, to eliminate the TDS component altogether. For W(100) in Fig. 3, the peak counting rate along the truncation rod is plotted, including the TDS contribution.

The expected functional form of the truncation rod in Eq. (2) is plotted as a dashed line in Figs. 1—3. The height has been adjusted in an attempt to fit the data, since these are not on an absolute scale. Although it does have the right concave shape, it clearly is an inadequate detailed description of the observations: the experimental intensity is more concentrated near to the Bragg points than expected. It is expected from the qualitative reasoning above that a broadened interface region between the crystal and vacuum would explain this general behavior. We will now build a model of surface roughness that explains the observations very well.

If a *partial* layer of atoms is added to the surface, in such a way that they occupy sites that are a continuation of the bulk lattice, there will be interference between the two-dimensional diffraction pattern of the layer and the ideal truncation rods of the rest of the crystal. Addition of a full layer, of course, has no effect as it simply offsets the starting value of the summation in Eq. (1). A convenient way to model roughness that extends to more than one layer is shown pictorially in Fig. 5. A fractional occupancy β (with $0<\beta<1$) is given to the first added layer, β^2 to the second, and so on. The distribution of atoms within each layer is not necessarily random, so this description would apply to terraced structures also, provided the lateral extent of the terraces is small compared with the coherence length of the x rays. The sums over j_1 and j_2 in Eq. (1) are unchanged since all the added atoms are assumed to be on lattice sites, so the diffracted intensity becomes

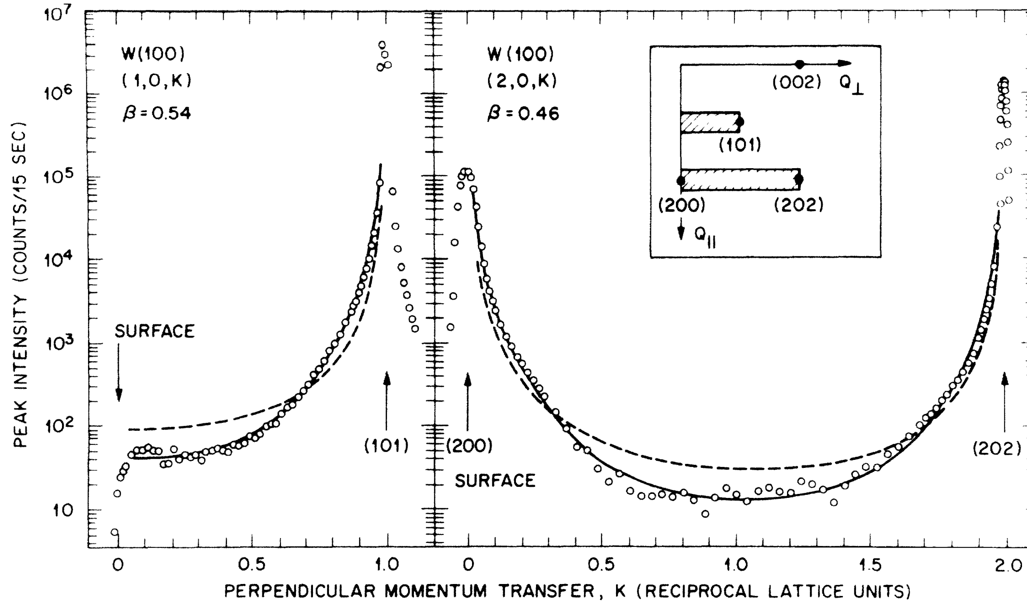

FIG. 3. Crystal truncation rods for W(100) in ultrahigh vacuum. The sample was prepared by repeated cycles of sublimation at 2500 K (passage of a current of 250 A for a few seconds) and burning in oxygen at a somewhat lower temperature (Ref. 5). Measurements were made with a rotating anode source and four-circle diffractometer. Peak intensity (not integrated) along the rod is shown for two orders of diffraction along the same azimuth as the shaded bars in the reciprocal space diagram show. Fits of Eq. (3) (solid line, with roughness) and Eq. (2) (dashed line, no roughness) are superimposed. The roughness parameter β was fitted independently for the two diffraction orders.

$$|F'(2\pi h/a_1, 2\pi k/a_2, q_3)|^2 = N_1^2 N_2^2 \left| \sum_{j=-\infty}^{0} \beta^{-j} e^{iq_3a_3j} + \sum_{j=1}^{\infty} \alpha^j e^{iq_3a_3j} \right|^2$$

$$\to N_1^2 N_2^2 \frac{(1-\beta)^2}{[1+\beta^2-2\beta\cos(q_3a_3)]} \frac{1}{4\sin^2(\frac{1}{2}q_3a_3)} \quad \text{as } \alpha\to 1 \text{ for } q_3a_3 \neq 2\pi l \,. \qquad (3)$$

The use of an attenuation parameter $0<\alpha<1$ in the second sum is justified because the beam has finite penetration into the crystal. If the far side of the crystal were not terminated gently (for example by a sum to a finite N_3), it too would give rise to a truncation rod. However, since $(1-\alpha) \ll (1-\beta)$ in practice, the form of Eq. (3) becomes independent of the value of α so that the limit $\alpha \to 1$ is valid. The functional form is dominated by the *sharper* of the two boundaries, so is given by the value of β in this case.

The result of including roughness in the calculations thus corresponds to multiplication of the scattering profile in Eq. (2) by a q_3-and β-dependent factor with a magnitude between zero and one. The rough truncation rod always lies lower in intensity than the smooth one, with the biggest proportional difference being halfway between the Bragg positions; the two curves converge as q_3 approaches the Bragg value, $2\pi l/a_3$. The modifying factor has a functional form similar to that which is commonly used to explain scattering from systems with partial stacking disorder:[2,7] it is broadly peaked at the Bragg nodes, with a shape that is controlled by the value of β. In the limit of a sharp interface, when β tends to zero, Eq. (3) becomes the same as Eq. (2). When β tends to unity corresponding to a gradual or very rough interface, the truncation scattering profile tends to $(\sin\frac{1}{2}qa)^{-4}$ but its amplitude vanishes. Intermediate values of β give profiles that are sharper near the Bragg nodes than $(\sin\frac{1}{2}qa)^{-2}$, but always less so than $(\sin\frac{1}{2}qa)^{-4}$.

Figure 1 shows the best least-squares fit of Eq. (3) to the Pt(111) crystal truncation rod. A roughness parameter $\beta=0.65\pm0.1$ was used with the fit being visibly worse at the limits of the error bar. Since the measurements were not on an absolute scale, and since the active area of the sample changes over the wide range of this scan (in which the scattering angle varies from 40° to 80°), a q-dependent scale factor, with a constant term and one linear in q, was simultaneously fit. This latter term also partly accounts for the form factor of the Pt atoms and for the Debye-Waller factor that is due to thermal motions in the crystal. Higher-order corrections to the scale factor were found to improve the fit slightly but did

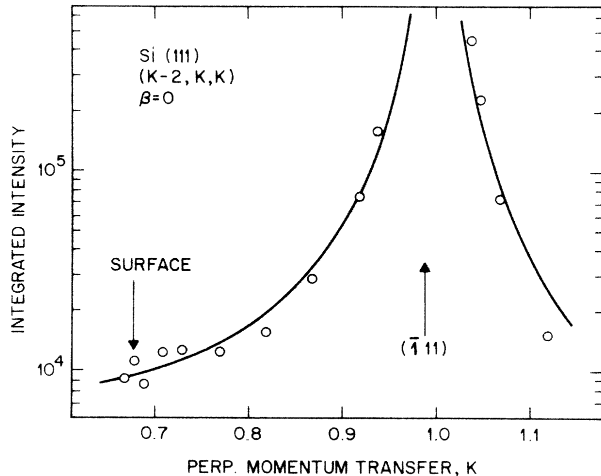

FIG. 4. Crystal truncation rod for Si(111) in ultrahigh vacuum, prepared by sublimation at 1450 K and slow cooling to 1000 K (Ref. 4). Measurements were made at SSRL using focused wiggler radiation of wavelength 1.738 Å and a four-circle diffractometer. Each point is integrated over its rocking curve and background subtracted. The rod shown is the same as the upper panel of Fig. 2 extending somewhat further and has a fit of Eq. (2) superimposed.

not affect the value of β; no attempt was made to interpret them further.

Figure 2 shows the same procedure applied to the InSb(111) data. The two sections of rod are related by inversion symmetry in the crystal and so can be juxtaposed (see Fig. 2 inset). They were simultaneously fit by Eq. (3) with a roughness of $\beta=0.40\pm0.05$. Figure 3 shows the fit to the W(100) data, where $\beta=0.54\pm0.15$ and $\beta=0.46\pm0.1$ result from independent fits to the different diffraction orders of truncation rods shown. The fit here is to the peak intensity along the ridge of the rod (as opposed to the integrated intensity); nevertheless the agreement is still very good, although the quoted values of β may be artificially reduced by TDS contamination of the data, which has not been subtracted. TDS has a basic q dependence given by the functional form of Eq. (2), but the variation of scale factor would be very different from that of the truncation rod, for reasons given above. It is clear in both the InSb(111) and W(100) cases that Eq. (3) is a much better fit to the observations than Eq. (2), and consequently that a roughened description of the surface is more suitable than a perfectly sharp one.

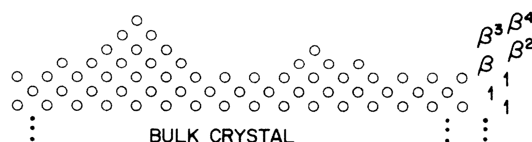

FIG. 5. Lattice model of a rough surface. Fractionally occupied layers reside above the topmost complete layer of atoms. The occupancies, marked on the right-hand side, follow an exponential distribution. The example here has $\beta=0.5$.

Contrasting behavior is seen, however, for Si(111) in Fig. 4. The data are not as accurate as our previous examples, but are fit reasonably well by Eq. (2), or equivalently by Eq. (3) with $\beta=0$. An error bar of ±0.3 accounts for the range of β over which Eq. (3) describes the data. Thus we have one example of a surface which is truly flat over the 2500 Å coherence length of the x-ray source used.

The model of roughness shown in Fig. 5 was chosen for simplicity, rather than for any physical reason. The distribution of layer occupancy was chosen to be exponential and was found to work quite well. Other distributions would give different functional forms for Eq. (3) but would all have the same qualitative behavior of concentrating the $(\sin\frac{1}{2}qa)^{-2}$ intensity [Eq. (2)] towards the Bragg points and away from the zone center. It is not clear that different detailed models of roughness could be distinguished at this level of accuracy. One central concept to *all* descriptions of crystal truncation rods, however, is the continuation of the crystal *lattice* into the roughened region. All these measurements were made at large momentum transfer, far from the small-angle region; we therefore strictly limit the description of roughness to that of an envelope function applied to a well-defined lattice. These measurements are therefore completely insensitive to the presence of any liquid or disordered layers on the surface of the crystal.

We should be careful to distinguish between roughness measured at zero and nonzero momentum transfer. Deviations from the Fresnel reflectivity curve[8] close to zero momentum transfer are also interpreted in terms of surface roughness. These roughness values, however, relate to the electron density boundary averaged over both in-plane directions and projected onto the surface normal. It is possible to conceive of both extreme situations where one measurement would show a perfectly sharp boundary while the other indicated a rough one: a perfectly truncated crystal covered with "rough" liquid, or a rough lattice (as in Fig. 5) which is "filled in" with amorphous material of the same density until its physical surface is smooth.

The lattice occupancy description is very general in one sense: the "occupancy" could refer to a static situation of random vacancies and adatoms on the surface or to a distribution of steps bounding terraces, as Fig. 5 suggests. It could, however, also describe the dynamic situation of a correlated liquid layer in which otherwise mobile atoms spend periods of time attached to lattice sites on the surface of a crystal. A third, more realistic manifestation of roughness would be that of surface enhanced vibration. Here the effective occupancy A_j of the jth layer would be given by an individual Debye-Waller factor[2] for the layer

$$A_j = e^{-2|q|^2\langle u_j^2\rangle}, \quad (4)$$

where q is the momentum transfer and $\langle u_j^2\rangle$ is the mean-square vibration amplitude of the atoms in the layers. If $\langle u_j^2\rangle$ were to increase uniformly towards the surface then the distribution of occupancies would indeed be exponential. This description is readily tested because of the predicted q dependence of the roughness parameter β. Our W(100) data have independent β values for the first- and second-order truncation rods, but the difference be-

TABLE I. Comparison of the four surfaces studied. Roughness β is taken from Figs. 1–4. σ_{rms} is calculated from Eq. (5). The roughness length scale is the inverse width of the crystal truncation rods measured in the plane of the surface. The reconstruction domain size is the inverse width of fractional-order reflections, when present.

Surface	Roughness β	Interplanar distance $d_\perp$ (Å)	rms roughness σ_{rms} (Å)	Roughness length scale (Å)	Reconstruction domain size (Å)	Instrumental coherence length (Å)
Pt(111)	0.65±0.1	2.27	5.2	150		150
InSb(111)	0.40±0.05	3.74	3.9	1000	1000	6000
W(100)	0.50±0.01	1.58	2.2	150	>100	150
Si(111)	0.0±0.03	3.14	0	2500	2000	2500

tween them is much too small for Debye-Waller effects to be the dominant contribution to roughness: if the first-order rod has $\beta_1=0.54$, then the second-order would have $\beta_2=(0.54)^4=0.09$ according to the description above; we find $\beta_2=0.46$.

It is conventional to express surface roughness as a root-mean-square elevation of the surface contour, σ_{rms}. We can convert the β values into σ_{rms} by calculating the second moment of the rigid lattice partial occupancy description of Fig. 5,

$$\sigma_{rms}=\frac{\beta^{1/2}}{(1-\beta)}d_\perp , \quad (5)$$

where $d_\perp$ is the lattice spacing perpendicular to the surface. This formula is specific to the model and will give an inaccurate measure of the surface contour if there are significant components of vibration or disorder. It should still be a useful parameter to represent the *ordered* component of the roughness on a length scale. Values of σ_{rms} are given for the four surfaces examined in Table I.

The lateral length scale over which the roughness is measured is also listed in Table I. This scale is given either by the coherence of the beam or by the lateral domain size of the crystal surface. In either case, it is measured by the width of the crystal truncation rod. This length is not necessarily related to the size of the reconstructed domains on the surface, also listed in Table I were appropriate, which is derived from the width of the fractional order peaks. It is reasonable that the crystal truncation rods are always seen to have characteristic lengths greater than or equal to the reconstruction domain size, because a reconstructed domain is presumably flat (see below). What is less clear, considering the description of Fig. 5, is how the roughness length scale can ever be less than the bulk domain size (resolution limited in each of our cases): InSb(111) shows a very large difference. The width of diffraction rods from terraced structures has been considered previously[9] and shown to oscillate as a function of the perpendicular momentum transfer. We believe that this effect, which is ultimately due to imperfect crystal orientation during polishing, is the explanation of our rod widths.

Roughness values are not believed to be fundamental properties of surfaces, and are more likely strongly related to the preparation conditions. This assumption was not tested here by variation of preparation, but has been demonstrated previously.[10] It should nevertheless prove interesting to apply this technique to systems in which roughening phase transitions are known to occur.[11] We can make certain general remarks on the σ_{rms} values in Table I. Firstly, the roughest surface, Pt(111), was the only sample not prepared using ultrahigh-vacuum protocols; and suggests that atmospheric chemical preparation methods[6] may not be as efficient as UHV ones from the point of view of roughness. Secondly, the smoothest surface, Si(111), which is within error of perfect flatness on the scale of 2500 Å, is well known to have extremely long coherence lengths of its reconstructed regions.[12] Moreover, since steps in this surface are seen directly in tunnelling microscope experiments[13] to interrupt the coherence between reconstructed regions on adjacent terraces, we know from the widths of the fractional-order reflections that these regions have to be flat over such distances.

Surface truncation rods must be considered in measurements of two-dimensional structure factors for surface structure determination. The main difficulty is their presence at positions that correspond to "1×1" surface peaks as Fig. 6 shows. The measured surface structure factor

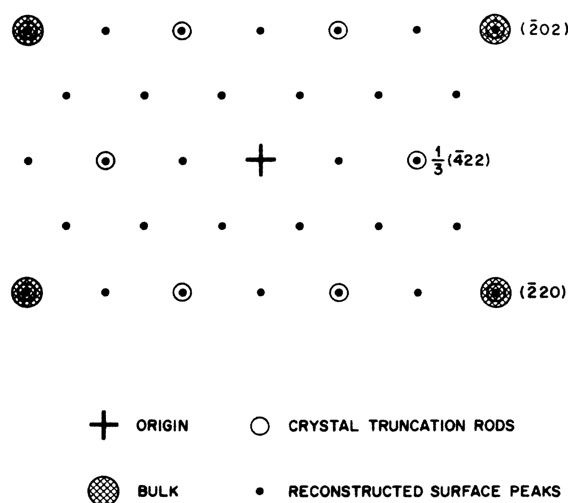

FIG. 6. The reciprocal lattice of a 2×2 reconstructed (111) face of a face centered cubic or diamond lattice crystal. The section shown is parallel to the face. A hierarchical classification of the reflections is shown. Reflections are indexed according to the bulk scheme; in the conventional definition of a surface reciprocal lattice (corresponding to a primitive hexagonal surface layer) the $\frac{1}{3}(\bar{4}22)$ position becomes the hexagonal (10) basis vector. The crystal truncation rods appear at the integer order positions in this hexagonal frame.

amplitude therefore has components both from the surface structure itself and from truncation of the bulk. Use of the measured amplitude in a Fourier calculation is further restricted because the truncation rod comes from the entire illuminated surface, while the corresponding surface structure component has contributions only from the ordered regions of the surface, which depend upon the level of contamination. In fact, very different time dependence (assumed to be due to contamination) of the intensities of integer-order and fractional-order peaks was observed in the case of the InSb(111)2×2 reconstructed surface.[3] All successful x-ray structure determinations of surfaces reported to date have omitted use of integer-order data.[1,3,4]

In principle, integer-order data can be used to great advantage, since Fourier amplitudes from the surface structure and the truncation rod would interfere with each other. The simplest case to consider is a substrate-overlayer system: fractional-order diffraction data from the overlayer alone can determine its *internal* structure but provides no information about its *registry* on the substrate; thus important information concerning the choice of site (e.g., hollow or atop) would not be available. Inclusion of the integer-order data could resolve that problem; the fraction of the surface area that is ordered would have to be included as an occupancy parameter in the analysis. Integer-order data could also play an important role in solving "registry" questions in reconstructed surface analyses. The structural analysis of InSb(111)2×2 left the registry question open,[3] the analyses of Au(110)1×2 and Ge(100)2×1 (Ref. 1) as well as Si(111)7×7 (Ref. 4) used heuristic determination of registry of the reconstructed layers on the bulk.

Finally, we would like to consider the possibility of using the crystal truncation rods for crystallographic phase determination. In most surface problems, an unknown surface structure lies on a face of a known bulk crystal structure. The ideal truncation rod structure factor can therefore be readily calculated both in amplitude and phase. The sign of the amplitude differences between the observed integer-order reflections and the values calculated from the bulk then relates to the size of the phase differences: if the surface and bulk add constructively (phase difference $<90°$) then the observed amplitude is greater than that calculated for the bulk, and *vice versa.* This method is formally analogous to the single isomorphous replacement method[14] or, equivalently, to the technique of holographic imaging. It could be used to obtain starting phase information as a precursor to model-independent structural refinement.

This experimental part of this work would have been impossible without the collaboration of J. D. E. McIntyre and W. Peck [Pt(111)]; R. Feidenhans'l, J. Bohr, M. Nielsen, M. Toney, and R. L. Johnson [InSb(111)]; M. Altman and P. J. Estrup [W(100)]; and W. K. Waskiewicz, P. H. Fuoss, J. B. Stark, and P. A. Bennett [Si(111)]. Valuable discussions with M. Nielsen, J. Bohr, and S. G. J. Mochrie are also acknowledged. S.S.R.L. is supported by the U.S. Department of Energy (Office of Basic Energy Sciences) and by the U.S. National Institute of Health (Biotechnology Resource Program). The work at HASYLAB was supported by the Danish Natural Science Foundation.

[1] I. K. Robinson, Phys. Rev. Lett. **50**, 1145 (1983); P. Eisenberger and W. C. Marra, *ibid.* **46**, 1081 (1981).

[2] B. E. Warren, *X-ray Diffraction* (Addison-Wesley, Reading, Mass., 1969).

[3] J. Bohr, R. Feidenhans'l, M. Nielsen, M. Toney, R. L. Johnson, and I. K. Robinson, Phys. Rev. Lett. **54**, 1275 (1985).

[4] I. K. Robinson, W. K. Waskiewicz, P. H. Fuoss, J. B. Stark, and P. A. Bennett (unpublished).

[5] M. Altman, P. J. Estrup, and I. K. Robinson (unpublished).

[6] A. Wieckowski, S. D. Rosasco, B. C. Schardt, J. L. Stickney, and A. T. Hubbard, Inorganic Chem. **23**, 656 (1984); J. D. E. McIntyre, W. Peck, and I. K. Robinson (unpublished).

[7] H. Jagodzinski, Acta Crystallogr. **2**, 201 (1949); J. M. Cowley, *ibid.* **A32**, 88 (1976); I. K. Robinson, in *The Structure of Surfaces,* edited by M. A. van Hove and S. Y. Tong (Springer-Verlag, Berlin, 1985).

[8] P. S. Pershan and J. Als-Nielsen, Phys. Rev. Lett. **52**, 759 (1984).

[9] M. G. Lagally, in *Chemistry and Physics of Solid Surfaces IV,* edited by R. Vanselow and R. Howe (Springer-Verlag, Berlin, 1982); P. Fenter and T. M. Lu, Surf. Sci. **154**, 15 (1985).

[10] G. Binnig, H. Rohrer, C. Gerber, and E. Weibel, Phys. Rev. Lett. **49**, 57 (1982); I. K. Robinson, Y. Kuk, and L. C. Feldman, Phys. Rev. B **29**, 4762 (1984).

[11] J. Lapujoulade, J. Perreau, and A. Kava, Surf. Sci. **129**, 59 (1983).

[12] M. Henzler, Surf. Sci. **132**, 82 (1983).

[13] R. S. Becker, J. A. Golovchenko, E. G. McRae, and B. S. Swartzentruber, Phys. Rev. Lett. **55**, 2028 (1985).

[14] D. M. Blow and M. G. Rossmann, Acta Crystallogr. **14**, 1195 (1961).

[15] A. M. Afanas'ev and M. K. Melkonyan, Acta Crystallogr. **A39**, 207 (1983).

[16] R. Feidenhans'l, J. Bohr, M. Nielsen, M. Toney, R. L. Johnson, F. Grey, and I. K. Robinson, in Festkörperprobleme XXV, 545 (1985).